Raman spectrum and phase transition in sodium azide*

George J. Simonis† and C. E. Hathaway
Department of Physics, Kansas State University, Manhattan, Kansas 66506
(Received 1 October 1973)

The Raman spectra of both the α and β phases of NaN_3 have been obtained and interpreted. The Raman-active E_g mode of the β phase splits into A_g and B_g modes as NaN_3 undergoes a phase transition at approximately 20 °C at atmospheric pressure. These phonons have been used to study the phase transition as a function of pressure and temperature. The temperature studies at atmospheric pressure were made over a range of 20 to 650 °K. The pressure studies were made for pressures ranging from 0 to 2.9 kbar for nine temperatures covering the range of 258 to 360 °K. The observed data are used to support an order-disorder transition model with a slightly disordered β phase. The contribution of the induced lattice strain to the phonon-frequency changes is shown by these data to dominate any contribution due to phonon coupling.

I. INTRODUCTION

Sodium azide, NaN_3, has a highly ionic lattice with one formula unit per primitive cell. The linear trinitrogen anion provides a simple variation on the extensively studied alkali-halide systems. Sodium azide is a relatively stable member of a family of sometimes violently unstable azide compounds. The instability of the azide ion allows the introduction of lattice defects at low temperature simply by irradiating the sample with ultraviolet light.[1] Azide-compound decomposition can be initiated by heat, shock, light, or ionizing radiation making temperature- and pressure-dependent spectral behavior of interest.

One of the most interesting aspects of the lattice dynamics of sodium azide is the occurrence of a temperature- and pressure-dependent structural phase transition of apparent higher-order character. The transition is known to be initiated with decreasing temperature near 20 °C,[2] and also can be induced by hydrostatic pressure.[3] The present work places emphasis on the pressure and temperature dependence of the Raman spectrum of sodium azide.

The space-group symmetry of the high-temperature phase of sodium azide, designated as β-sodium azide has been found by x-ray analysis to be $R\bar{3}m$ (D_{3d}^5) with one formula unit per primitive cell.[2-4] The β-sodium azide rhombohedral cell is illustrated in Fig. 1. The lattice structure of the β phase can be described in terms of the primitive rhombohedral cell or the nonprimitive hexagonal or monoclinic cells. The lattice parameters at 23 °C are given in Table I. There are nine optically active modes of which six are infrared active ($2E_u + 2A_{2u}$) and three are Raman active ($1A_{1g} + 1E_g$). Each of these modes may be classified as "internal" or "external" in character depending upon whether the predominant relative atomic motions are internal or external to the azide ion. The internal modes are the A_{1g} azide symmetric stretch mode, the E_u azide bending modes, and the A_{2u} azide asymmetric stretch mode. These modes are often referred to simply as ν_1, ν_2, and ν_3, respectively, because of their similarity to the molecular vibrations. The external modes are the E_u and A_{2u} azide translations and the E_g azide librations. It should be noted that these verbal descriptions are intended only to be conceptually helpful. They are not rigorous descriptions of the phonons in the lattice. The Raman-scattering-intensity matrices obtained from the conventional Raman-scattering tensors[5] are shown below:

$$A_{1g}: \begin{bmatrix} a^2 & 0 & 0 \\ 0 & a^2 & 0 \\ 0 & 0 & b^2 \end{bmatrix}, \quad E_g: \begin{bmatrix} c^2 & c^2 & d^2 \\ c^2 & c^2 & d^2 \\ d^2 & d^2 & 0 \end{bmatrix}.$$

Several studies of the β-sodium azide optical spectra have been conducted and extensive assignment of the spectral features has been presented.[6-9] A lattice dynamical calculation based on measured $\kappa = 0$ optical frequencies has also been made.[10] Unfortunately, sufficiently large single crystals have not been available for an inelastic-neutron-scattering determination of the dispersion curves. Only neutron scattering from powdered samples has been studied.[10]

The low-temperature phase, designated as α-sodium azide, has been determined to have space-group symmetry $C2/m$ (C_{2h}^3) with one formula unit per primitive cell.[2] This is a distorted rhombohedral cell which is to be distinguished from the monoclinic crystallographic cell with two formula units per crystallographic unit cell. The monoclinic cell presented in Fig. 1 is useful for visual-

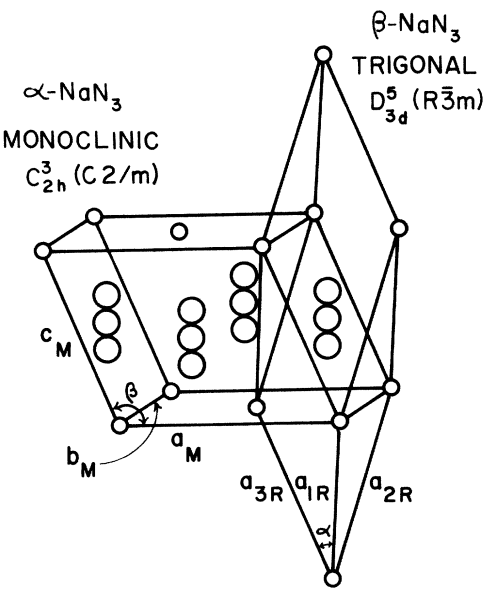

Fig. 1. α- and β-sodium azide crystallographic cells showing their correspondence in the β-phase.

izing the transition. The monoclinic cell parameters at $-95\,^{\circ}C$ are given in Table I. The optical-mode symmetries and their correspondence with the modes of β-sodium azide are listed in Table II. The infrared or Raman activity of the modes is not affected by the structural change but the details of the Raman tensors are.

The phase transition can occur in any one of three equivalent directions and probably varies from point to point within a crystal. For this reason the α-sodium azide scattering intensity matrices are presented with an arbitrary rotation θ of the crystallographic axes about the z direction relative to the sample axes. Sample X and Y axes refer to an arbitrarily selected but uniquely defined pair of orthogonal axes in the X-Y plane of a given sample. Sample axes will be understood to apply unless otherwise stated:

$$A_g:\begin{bmatrix} (a\cos^2\theta + b\sin^2\theta)^2 & \left(\frac{(a-b)\sin^2 2\theta}{2}\right)^2 & d^2\cos^2\theta \\ \left(\frac{(a-b)\sin^2 2\theta}{2}\right)^2 & (a\sin^2\theta + b\cos^2\theta)^2 & d^2\sin^2\theta \\ d^2\cos^2\theta & d^2\sin^2\theta & c^2 \end{bmatrix},$$

$$B_g:\begin{bmatrix} e^2\sin^2 2\theta & e^2\cos^2 2\theta & f^2\sin^2\theta \\ e^2\cos^2 2\theta & e^2\sin^2 2\theta & f^2\cos^2\theta \\ f^2\sin^2\theta & f^2\cos^2\theta & 0 \end{bmatrix}.$$

The above dependence on θ is in contrast to the β-phase matrices which are left unchanged by such a rotation θ.

The space groups of α- and β-sodium azide are both symmorphic, allowing the symmetry discussion to be conducted in terms of the appropriate point group operations. The transition from the β to the α phase involves a reduction by a factor of 3 in the number of point group symmetry elements as indicated in Table III. Therefore, according to Landau's group-theoretical considerations,[11] this transition will have nonzero third-order terms in the expansion of the thermodynamic potential and, consequently, can not be strictly of second order.

Pringle and Noakes[2] have conducted a temperature dependent x-ray study of the transition. They find the β-to-α transition to involve a shearing of the sodium layers in such a way that the monoclinic cell β angle decreases with decreasing temperature. At the same time a corresponding but disproportionately large tilt of the azide ion occurs in the reflection plane of the monoclinic cell such that the azide ion comes closer to two nearest-neighbor sodiums than to the other four. Other lesser changes occur simultaneously. Pringle and Noakes reported the transition to be predominantly second order in character since these changes begin at $18\,^{\circ}C$, proceed continuous-

TABLE I. Unit-cell parameters for α- and β-sodium azide.[a]

	a (Å)	b (Å)	c (Å)	Cell angle
β-phase (23 °C), $R\bar{3}m$				
Rhombohedral	5.491	...	...	$\alpha = 38.7°$
Hexagonal	3.646	...	15.213	
Monoclinic	6.316	3.647	5.493	$\beta = 112.6°$
α-phase (−95 °C), $C2/m$				
Monoclinic	6.211	3.658	5.323	$\beta = 108.43°$

[a] Values taken from Refs. 2, 16, and calculations based on their results.

ly as a function of decreasing temperature, and are not yet completed at $-100\,^{\circ}C$. Their transition temperature T_c compares favorably with values between 19 and 22 °C obtained by other authors.[12,13] They find the splitting of formerly degenerate plane spacings to follow the proportionality

$$[(d_1 - d)/d]^2 \propto T_c - T, \quad (1)$$

where d represents the degenerate plane spacing; d_1 and d_2 represent the split nondegenerate plane spacing. Figure 12 presents some of the results upon which this statement is based.

Fritzer and Torkar[14] observed only a very slight increase in the heat capacity in the vicinity of 20 °C. The only conclusion that they were able to draw was that no pronounced structural change could occur because no sharp deviation in the heat capacity was observed. A similar conclusion was reached by Campbell and Coogen[15] based on their NMR measurements.

Bradley, Grace, and Munro[3] demonstrated that the transition could also be caused by applying pressure. Pringle and Noakes[2] observed a temperature-pressure correspondence of 35 bar/°C, with regard to induced effects, upon comparing their results with those of the pressure study. No actual lattice-cell-parameter values as a function of temperature or pressure have been determined except for the Pringle and Noakes[2] studies at 23 and $-95\,^{\circ}C$, and those of Stevens and Hope[16] at 23 °C. Based upon the observed correspondence between temperature and pressure changes, one also would expect to find lattice plane spacing changes to be proportional to $(P-P_c)^{1/2}$.

Pringle and Noakes[2,17] find the phase-transition behavior to be consistent with an order-disorder mechanism in which the librational motion of the azide ion is visualized as involving a process of jumping between three tilted azide potential minima. This model is supported by their observation of an apparent larger diameter for the azide ion at its extremities over that of the central nitrogen in the β phase. The β-phase symmetry is preserved in their model only insofar as equal populations of the three tilted orientations exist. The β- phase–to–α-phase transition then is pictured as involving a population increase of two of the orientations at the expense of the third with a resultant tilt in the average azide ion orientation.

TABLE II. Correspondence between the $\vec{k}=0$ lattice vibrational modes of α- and β-sodium azide.

$R\bar{3}m$	$C2/m$	Description [a]
Acoustic modes		
E_u	A_u	Cell translation parallel to $\hat{y}_M$
	B_u	Cell translation parallel to x_M
A_2	B_u	Cell translation parallel to z_M
Optic modes		
Infrared active		
E_u	A_u	Atomic displacements parallel to $\hat{y}_M$
	B_u	Atomic displacements parallel to $\hat{x}_M$
A_{2u}	B_u	Atomic displacements parallel to $\hat{z}_M$
E_u	A_u	N_3 bending in $(YZ)_M$ plane
	B_u	N_3 bending in $(XZ)_M$ plane
A_{2u}	B_u	N_3 asymmetric stretch
Raman active		
E_g	A_g	N_3 libration in $(xz)_M$ plane
	B_g	N_3 libration in $(yz)_M$ plane
A_{1g}	A_g	N_3 symmetric stretch

[a] The Cartesian coordinates are defined for the monoclinic unit cell.

II. EXPERIMENTAL

The sodium azide crystals used in these measurements were grown by very slow diffusion of methanol into a saturated water solution at constant temperature. The crystals obtained were in the form of platelets as thick as 1 mm with faces as large as 5 cm^2. The samples had undulating surfaces and some visible flaws. X-ray Laue backscattering studies indicated that the samples were untwinned single crystals. The crystalographic z axis was found to be normal to the faces.

Natural crystal faces and cleaved edges were used for entrance and exit optical surfaces for almost all of the measurements. However, it was found that good optical surfaces could be obtained by polishing first with a slightly water-moistened polishing cloth followed by a similar procedure with acetone.

The Raman measurements were made predominantly with the 4965-Å argon-ion laser line. Several other lines of an argon-ion laser and the 6328-Å line of a helium-neon laser also were used. The detection and photon-counting apparatus employed has been previously described by Temple and Hathaway[18] and by Hathaway and Rahn.[19]

The optical pressure cell used was designed by

TABLE III. The point-group symmetry operations of α- and β-sodium azide and their correspondence.

$\bar{3}m$	E	C_3^1	C_3^2	C_2	C_2'	C_2''	i	S_6^1	S_6^5	σ_d	σ_d^1	σ_d^{11}
$2/m$	E	|	|	C_2	|	|	i	|	|	σ_h	|	|

Stanley Robertson Fort Hays Kansas State College, and is illustrated in Fig. 2. The cell was constructed of 4041 tool steel, heat treated to a Rockwell C45–48 hardness. The windows were single-crystal sapphire. The pressure was generated by a hydraulic hand pump and delivered to the sample chamber by means of Octoil-S fluid in which the sample was immersed.

The pressure was indicated with an accuracy of ± 500 lb./in.^{2} by means of an American Instrument Co. calibrated pressure gauge. The measured pressure values were converted to kbar. The sample temperature was measured with a calibrated 40 Driver-Harris Alloy No. 121-122 thermocouple placed in direct thermal contact with the sample and approximately 3 mm from the point of focus of the laser. The thermocouple leads were passed into the cell through a length of high-pressure tubing filled with epoxy to make a pressure-tight seal.

Pressure-cell temperatures from room temperature to 87 °C were maintained to better than ± 0.25 °C by means of an external heater surrounding the cell and a temperature controller. Cell temperatures from room temperature to − 15 °C were maintained to within ± 0.5 °C by means of thermoelectric coolers placed in thermal contact with the exterior of the cell.

Measurements were made from room temperature to 20 °K at 0 kbar by means of a liquid-nitrogen Dewar with a counterbalancing sample heater, and with a Joule-Thomson hydrogen-gas Dewar. Zero-pressure measurements were made from room temperature to 675 °K by means of a heater mounted in an evacuable glass chamber. Temperature stability of better than ± 2 °K was readily obtainable with the Dewar and the heater systems.

A least-squares-fitting program was used to obtain individual line-shape parameters from data containing overlapping bands. This program also allowed minimization by a deconvolution technique of instrument and laser linewidth effects on the data. This technique involved fitting the data with a convolution of Lorentzian line shapes, a linear sloping background, and an instrument function. The instrument function was obtained by scanning over the laser line with the same instrument settings as those used in the original measurement. Confidence intervals for the fit parameters were calculated as a function of individual data point uncertainties, assuming Poisson statistics for the photon counts. Goodness-of-fit parameters χ^2 were also determined.[21]

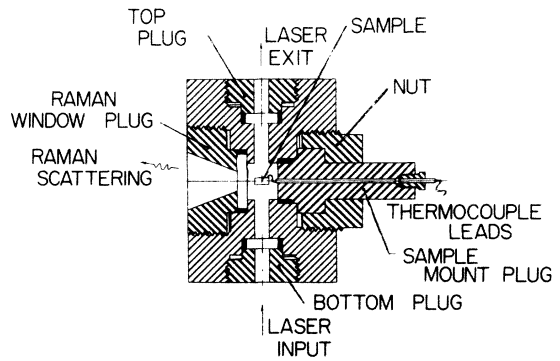

FIG. 2. Optical hydrostatic pressure cell with sapphire windows.

III. RESULTS AND DISCUSSION

A. β-sodium azide

The Raman spectrum of β-sodium azide has been reported by Bryant[7] as consisting of lines at approximately 122, 1267, and 1358 cm^{-1}. The present work presents considerable additional detail not previously reported. The survey spectrum, as recorded in this work is given in Fig. 3. The peak positions and full widths at half-maxima are presented in Table IV.

Normalized scattering intensity matrices of the three dominant features of the β-sodium azide spectrum are as follows:

$$121\ \text{cm}^{-1}: \begin{pmatrix} 7 & 7 & 96 \\ 7 & 7 & 100 \\ 96 & 100 & 43 \end{pmatrix},$$

$$1266\ \text{cm}^{-1}: \begin{pmatrix} 2 & 1 & 2 \\ 1 & 2 & 2 \\ 2 & 2 & 100 \end{pmatrix},$$

$$1358\ \text{cm}^{-1}: \begin{pmatrix} 7 & 0 & 2 \\ 0 & 7 & 1 \\ 2 & 1 & 100 \end{pmatrix}.$$

The 121-cm^{-1} measurements presented here were made at 100 °C in an attempt to reduce perturbations that might occur in the vicinity of the phase transition. However, similar results were obtained at 25 °C except for a slight increase in the relative size of the XZ, YZ, ZX, and ZY elements. Since the elements of these matrices are not changed by an arbitrary rotation θ about the z axis in the β phase, it was not necessary to orient the sample in the X-Y plane to obtain polarization data.

The matrix elements are averages of measurements involving several appropriate crystallographic orientations and several points within a sample. These matrices are only meant to be indicative of the polarization characteristics. Inconsistencies in relative intensity were observed between specific sets of measurements. These variations are probably due to sample imperfections, multiple internal reflections within the thin platelets, finite solid angle of the entrance and exit radiation, and uniaxial crystal effects. The two refractive indices of β-sodium azide are substantially different with $n_{\parallel}=1.72$ and $n_{\perp}=1.37$.[20]

The 120-cm^{-1} line is readily assigned as the E_g azide librational mode because it is the only low-frequency line of significant intensity. Its matrix elements are in good agreement with those expected for an E_g mode except for the ZZ element. It is difficult to explain the nonzero ZZ element as caused by the problems previously mentioned. Changing the f number of the collection optics made no significant difference in the relative size of the ZZ element. The other matrix elements are consistently observed to be substantially smaller than the ZZ element even though the ZZ element is required to be zero by symmetry while no other elements are. Very good polarization ratios were obtained for the high-frequency lines.

Figure 4 presents typical polarization data for the librational mode at 25 °C. The nonzero ZZ element is more understandable if one adopts a disorder model for the high-temperature phase of sodium azide. The smooth curve through the $X(ZX)Y$ data points is a least-squares single Lorentzian fit to the data.

The narrow 1358-cm^{-1} band of A_{1g} symmetry dominates the high-frequency spectrum. We also observed this line in an unsaturated water solution at a reduced frequency of 1340 cm^{-1} with a half-width of 12 cm^{-1}. It has been assigned therefore as the only high-frequency first-order Raman active mode, the azide symmetric stretch.

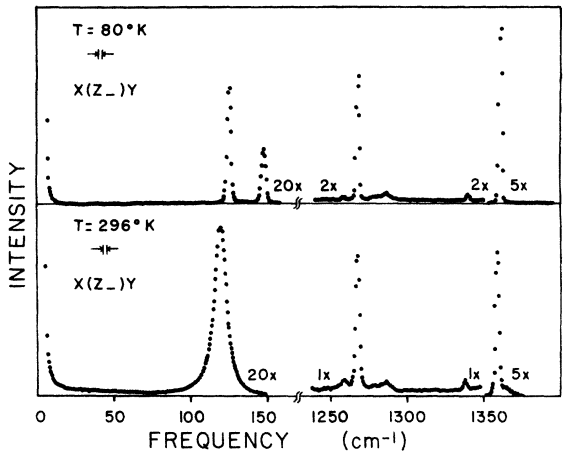

FIG. 3. Survey spectrum of α-sodium azide (80 °K) and β-sodium azide (296 °K) at 0 bar.

The 1266-cm^{-1} line is approximately twice the reported 638-cm^{-1} frequency of the internal azide bending mode.[7] Its half-width is relatively narrow as would be expected. We also observed it in an unsaturated water solution of sodium azide, although mixed with the 1358-cm^{-1} line, with the maximum occurring at approximately 1255 cm^{-1}. It is assigned as the bending mode overtone. Its large intensity and slight frequency discrepancy is believed to be caused by Fermi resonance with the A_{1g} azide symmetric stretch mode.

The other observed features of the spectrum are not as easily assigned. The broad weak band at 255 cm^{-1} is not observed at low temperatures and is believed due to higher-order phonon scatter-

TABLE IV. Peak positions and full widths at half-maxima.

α-sodium azide		β-sodium azide			
88 °K		297 °K		650 °K	
ν (cm^{-1})	γ (cm^{-1})	ν (cm^{-1})	γ (cm^{-1})	ν (cm^{-1})	γ (cm^{-1})
125.3 ± 0.5	0.7 ± 0.2	121.0 ± 0.5	8.3 ± 0.4	104 ± 1	24 ± 1
148.4 ± 0.5	0.8 ± 0.2				
Not observable		255 ± 5	25 ± 8		
1259 ± 1.5	1.5 ± 1	1258 ± 1.5	2.5 ± 1		
1268 ± 1.5	0.3 ± 0.2	1266 ± 1.5	1.1 ± 0.4	1263 ± 1.5 [a]	4.0 ± 0.5
1275 to 1290	b	1270 to 1290	b		
1339 ± 1.5	0.7 ± 0.4	1336 ± 1.5	0.9 ± 0.3		
1360 ± 1.5	0.3 ± 0.2	1358 ± 1.5	1.2 ± 0.3	1354 ± 1.5	6.0 ± 0.5
Not observable		1364 ± 1.5	b	1363 ± 2	b

[a] Measured at 523 °K.
[b] Not available.

ing or possibly the Raman-forbidden LO(A_u) azide translation.[9] The band maxima observed at 1258 and 1336 cm^{-1} correspond very well with $N^{15}NN$ linear-triatomic-oscillator isotope-shifted frequencies calculated to be 1259 and 1335 cm^{-1}. The half-widths at low temperature also are consistent with such an assignment. The relative isotopic abundance of N^{15} is 0.37% leading to predicted intensity ratios between the pure and isotope shifted lines of 0.7%. The observed ratios at low temperature were 1%. Lines with essentially the same frequency shift from ν_2 as that of the 1268-cm^{-1} line have been observed in KN_3,[22] CsN_3,[23] and AgN_3.[24] A line similarly corresponding to the sodium azide 1335-cm^{-1} line has been reported in AgN_2.[24] Bryant[7] has conducted infrared absorption measurements on pressed KBr disk samples containing $NaN^{15}NN$ enriched to 95%. He observed the isotope shifted bending mode at 628 cm^{-1} leading to an isotope overtone frequency to 1256 cm^{-1}. Isotope lines have also been observed in KNCS,[25] confirming the presence of such lines in a lattice with bonding similar to that of the alkali azides.

These observations are not conclusive because arguments also can be raised against such assignments. The Fermi resonance involved for the 1266-cm^{-1} line also applies to the isotope-shifted line yielding a value of 1246 cm^{-1} for the isotope overtone as calculated from Bryant's infrared absorption measurements on the bending mode. This value is 12 cm^{-1} below the observed line. The relative intensity of the 1258-cm^{-1} line increases with temperature to more than 5% as compared to the 1266-cm^{-1} line at room temperature as well as acquiring an irregular shape. However, this could be caused by a low-frequency wing on the 1266-cm cm^{-1} line generated by anharmonic effects. A problem more difficult to explain is the absence of an isotope-shifted bending mode overtone due to $NN^{15}N$. This line is calculated to be at 1238 cm^{-1} with 0.3% of the intensity of the 1266-cm^{-1} line. No such line was observed. However, it should be noted that Bryant[6] also did not report such a line in his isotope enriched samples. Bryant did assign a band observed at 1350 cm^{-1} as the isotope-shifted ν_1 frequency. He indicated that this assignment was confirmed using isotope enriched samples of 95% $NaN^{15}NN$. No line was observed at that frequency in the present work.

The structure of the 1270- to 1290-cm^{-1} band, presented in Fig. 5, resembles that of second-order Raman scattering processes. This band is believed to be caused by coupling between the azide bending modes and the external lattice phonons or coupling between azide ions. It is of interest to note that potassium azide, cesium azide and silver azide all have a set of four lines in the $2\nu_2$ region of the spectrum similar in position and relative intensity to those of sodium azide. This is true even though the respective point groups are D_{4h}, D_{4h}, D_{2h}, and D_{3d}, respectively. The first three azides have two formula units per primitive cell and orthogonal axes for neighboring azides, while sodium azide has one formula unit per primitive unit cell and all azide axes parallel. The structural phase transition that occurs in sodium azide also has negligible effect on these lines.

The 1364-cm^{-1} band is believed to be different in origin as evidenced by its very strong temperature dependence. It is unobservable at 88 °K but

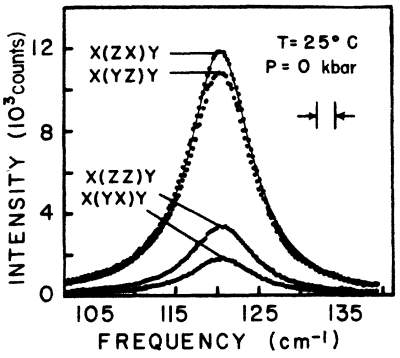

FIG. 4. Typical polarization data for the E_g librational mode. The solid line is a one Lorentzian least-squares fit to the $X(ZX)Y$ data.

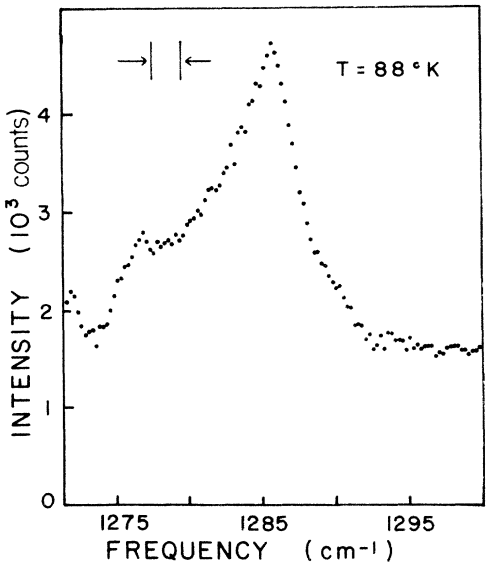

FIG. 5. Weak high-frequency band whose structure resembles that of second-order scattering processes.

increases asymptotically to half the intensity of the ν_1 line at 650 °K. Corresponding lines have been observed in potassium and cesium azide.[26] Despite the striking similarities between the high-frequency spectra of the various azides, diverse assignments have been made by various authors. It appears likely that there is a common explanation for the lines observed in the four different azides.

B. α-sodium azide

The infrared and Raman spectra of α-sodium azide are very similar to the spectra of β-sodium azide if allowance is made for normal anharmonic effects. This is attested to by Bryant's[7] assignment of the features of both spectra without acknowledging the existence of the α-β structural phase transition.

The one conspicuous exception to this over-all similarity is the frequency splitting of the formerly degenerate E_g librational modes into an A_g and a B_g mode. This splitting was first reported by Temple[27] as a function of temperature, and by Simonis[28] as a function of pressure.

The frequency exhibiting the largest change with temperature is assigned as the A_g mode because the A_g mode displacements match most closely the lattice distortion of the phase transition, and the A_g mode also has the decreasing nearest-neighbor sodium distance in its plane of oscillation.

As observed earlier, domains of differing orientation are likely to occur in the α-phase. This is consistent with the polarization variations observed in the scattering from point to point within a given crystal. A complete scattering matrix study therefore could not be conducted. However, it was possible to use the polarization character at a single point in the crystal to enhance first one line and then the other in order to better resolve the individual lines. Typical polarization data are presented in Fig. 6. The smooth curves are least-squares fits to the data obtained as described above.

The polarization separation was found to be the greatest for $Z(\ )Y$ sample orientation. The polarization separation was often maintained for repeated recycling through the transition. The optimum polarizer settings were found to be 90° apart but bore no consistent relationship to the direction of propagation of the exit beam. Although not clearly understood, it was observed that polarization analyzer adjustments had negligible effect on on the relative intensities of the two lines. Therefore, no analyzer was used in order to maximize signal intensity.

The ZZ element of the B_g-mode scattering matrix theoretically should be zero for arbitrary rotation of the X and Y crystallographic axes as discussed earlier. Experimental measurements consistently yielded ZZ matrix elements which were 20% or more of the largest matrix element YZ. Multiple domains in the sample in the α-phase are likely to add to the difficulties discussed earlier in relation to β-sodium azide polarized scattering, but are not believed to provide a complete explanation.

No observable perturbations occur in the high-frequency spectrum that can be attributed to the phase transition. This is particularly significant with regard to the 1268-cm^{-1} line which might be expected to be split by the lower symmetry of the azide site in the α-phase. A splitting of as little as 0.5 cm^{-1} would have been readily detectable at 20 °K. This lack of observed splitting is indicative of the small effect that the lattice has on the internal modes of the azide ion.

C. Pressure-dependent Raman studies

Pressure range of the cell employed in these measurements was not sufficient to allow a pressure-dependent study of the changes in the internal-mode frequencies. However, the pressure-induced changes in the librational-mode frequencies were readily observable and were studied extensively. These bands were studied as a function of pressure at nine temperatures ranging from −15 to 87 °C. Figure 7 presents the pressure-dependent frequency behavior obtained for three of these temperatures. The symbol size is approximately representative of the uncertainty in the frequency. Data were taken for ascending and descending pressure increments and also for various relative intensities of the two peaks. All peak position data appear to be consistent within

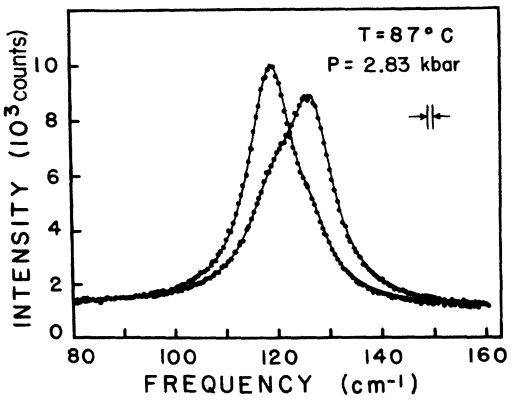

FIG. 6. A_g and B_g librational-mode polarization separation. The solid lines are two Lorentzian least-squares fits.

the uncertainties of the measurements, with no detectable hysteresis effects.

The E_g mode exhibits normal anharmonic behavior, increasing linearly in frequency with increasing pressure at a rate of 1.1 cm^{-1}/kbar at 87 °C. The B_g mode exhibits similar behavior at a rate of 0.81 cm^{-1}/kbar at −15 °C. However, near the transition point the B_g frequency is an anomalously larger than the frequency as extrapolated from higher pressures would indicate. Without this nonlinear deviation in the frequency, there would be a discontinuity at the transition point. At low temperature the χ^2 values for the computer fits were consistently near 1.0 while for higher temperatures they exceed 2.0. This increase is believed to be caused predominantly by the increasing fractional contribution of the nonlinear background and the broader spectral region covered by the line. The one Lorentzian fits in the β-phase exhibit a deterioration of the χ^2 values several hundred bars before the transition occurs. This may be indicative of changes preceeding the extrapolated transition pressure P_c.

For $(P-P_c)$ less than 400 bar in the α-phase, the intensity of the A_g mode is observed to decrease significantly relative to that of the B_g mode for all samples, incident polarizations, and temperatures. The total integrated intensity of the two bands is found to be approximately constant throughout the pressure range including both sides of the transition point.

Figure 8 presents half-width data for three of the temperatures of the investigation. The half-widths, which might be expected to be sensitive to lattice peculiarities near the transition point, change in relative magnitude for the A_g and B_g modes within approximately 1.4 kbar of the transition point. Also, the A_g and B_g half-widths each consist of two distinguishable groups with different magnitudes corresponding to the two incident polarizations employed for the measurements. The over-all consistency between half-width determinations is observed to deteriorate in the

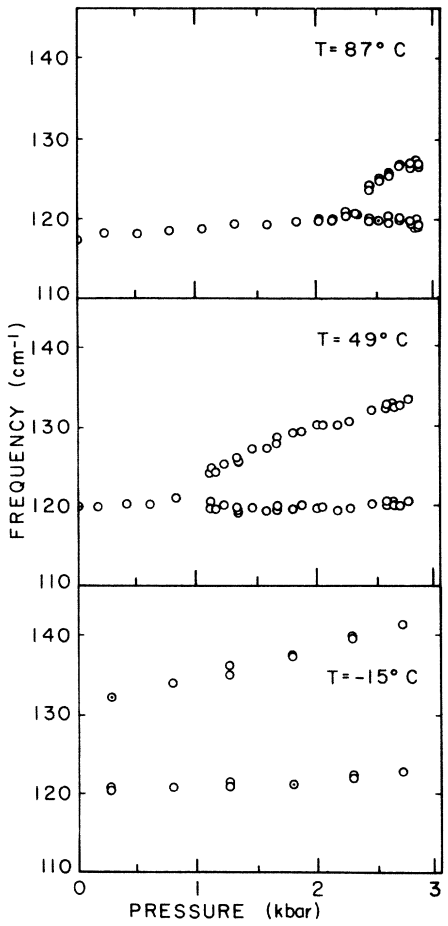

FIG. 7. Pressure-dependent librational-mode frequencies for three of the nine temperatures studied.

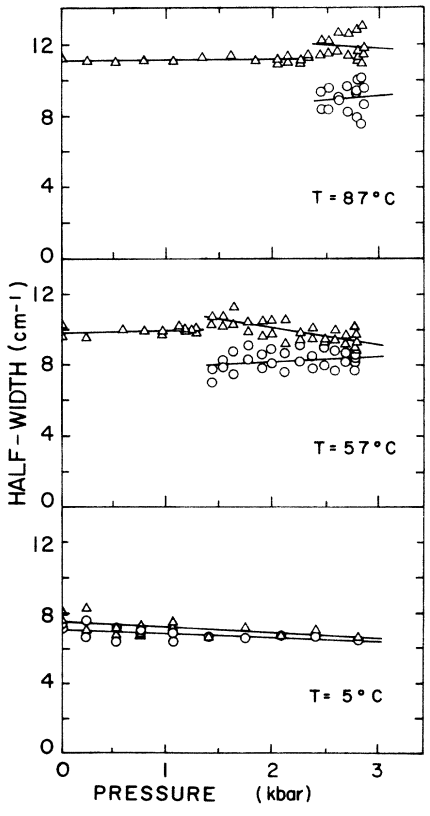

FIG. 8. Librational-mode pressure-dependent half-width data at several constant temperatures. Triangles represent the E_g and B_g librational modes. Circles represent the A_g librational mode.

α-phase near the transition point.

The symbol size is representative of the half-width estimated uncertainty for measurements in which the two lines do not overlap substantially or only one line is present. However, for small separations of the lines, the confidence contours in parameter space[21] increase in volume and take on more irregular shapes making uncertainties difficult to estimate. The "best-fit" parameter uncertainties in this region cannot be accurately determined nor can the region of anticipated difficulty itself be determined without an extensive investigation of these contours. Such an investigation is beyond the scope of the present work. It is therefore not clear at the present time whether the derived half-width behavior at and near the transition point is caused by peculiarities of the fitting procedure, physical effects, or a combination of the two. Diverse first guesses for the computer-fitting procedure were found to result in almost identical parameter values with any data for which convergence was obtainable. The agreement between the results of different measurements and different polarizations also gives some indication of the parameter uncertainties. Half-width changes definitely are only a small fraction of the total half-width to within 350 bar of the transition pressure.

As Fig. 7 illustrates, the splitting of the two librational mode frequencies has a nonlinear pressure dependence. Nevertheless, the behavior of these modes does not conform with that associated with soft modes, that is, modes which become unstable at the transition point. The most significant discrepancy is that no observed Raman-active mode frequency in the α-phase approaches zero as the transition point is approached, although the largest part of the lattice distortion occurs over several kbars of pressure change. According to Worlock's lemma,[29] the soft mode must be Raman active and totally symmetric in the low-symmetry phase. $SrTiO_3$[29] is an excellent example of a socond-order displacive phase transition exhibiting such a mode. Given the C_{2h} lattice symmetry of α-sodium azide, the A_g librational mode would be the most logical candidate for the soft mode. However, the atomic displacements do not match those of the phase transition as described by Pringle and Noakes.[2] Even if the lattice symmetry were incorrect, the soft mode should be observed in the α-phase and was not.

The other commonly recognized major type of second-order phase transition is the λ- or order-disorder transition. KNCS (Ref. 30) and the ammonium halides[31] are examples of this type of transition. For many such materials no single mode has been observed to approach zero as the second order transition point is approached. However, in disordered phase of both KNCS and the ammonium halides, the disruption of lattice translational symmetry manifests itself in the breakdown of the $k=0$ selection rule for first-order optical processes. Broad bands corresponding to the density of states curves then appear in the Raman spectra. No such behavior is observed in relation to the librational modes in sodium azide. The individual phonon half-widths and line shapes are well behaved in sodium azide throughout the transition region in contrast to those of some of the other order-disorder transition materials. Sodium azide does not obviously fit either of the standard second-order phase-transition models.

An attempt is made in this work to relate the observed frequency behavior to the lattice distortion using anharmonic-phonon theory. Starting with Cowley's description[32] of anharmonic perturbations on the harmonic phonon frequencies

$$\nu^2 = \nu_0^2 + 2\nu_0(\Delta_{TE} + \Delta_{AH}), \tag{2}$$

where Δ_{TE} is the frequency change linearly proportional to finite lattice strains $\eta_{\alpha\beta}$, and Δ_{AH} is the frequency change due directly to phonon coupling. The change due to phonon coupling is linearly related to phonon Bose-Einstein factors n_i.

Lattice strains may be introduced by applying pressure or by thermal expansion processes. The Bose-Einstein factors are changed, under normal circumstances, predominantly by temperature changes. Although this is not necessarily true in the neighborhood of phase transitions, we will assume it to be so based on the observed half-width data. Pressure and temperature-dependent studies of the strain and frequency behavior then allow one to separate the two effects. As Cowley shows, the phonon half-widths are closely related to the same population factors n_i that cause the changes in Δ_{AH}. Although the two relationships are not identical we will take the observed half-width behavior as an indication that

$$\Delta_{AH}(A_g) \simeq \Delta_{AH}(B_g) \tag{3}$$

for $P-P_c$ greater than 135 bar. It then follows that

$$\nu_{A_g}^2 - \nu_{B_g}^2 = 2\nu_0[\Delta_{TE}(A_g) - \Delta_{TE}(B_g)]. \tag{4}$$

As observed earlier, the x-ray measurements are consistent with

$$\eta_{\alpha\beta} \propto (P-P_c)^{1/2}, \tag{5}$$

although the measurements reported up to the present do not prove this proportionality. It then follows that

$$(\nu_{A_g}^2 - \nu_{B_g}^2)^2 \propto P - P_c. \tag{6}$$

The corresponding librational mode reduced data for the nine temperatures of the pressure study are presented in Fig. 9 along with weighted linear least-squares fits to the data. The parameters of these fits are presented in Table V along with parameter confidence intervals, χ^2 goodness of fit values, extrapolated phase transition pressures, and transition pressure confidence intervals. The χ^2 values are less than 1.0 without exception indicating the straight line parameter uncertainties are conservative values.

D. Temperature-dependent Raman studies

The temperature dependence of the azide internal modes is of special interest because the azide ion is the origin of the decomposition of azide compounds. Although the instability is believed to be electronic in origin,[33] it could affect the phonon optical spectra. Frequencies and half-widths of several high-frequency bands are given in Table IV for 88, 297, and 650 °K.

The 1358-cm^{-1}/1364-cm^{-1} line-intensity ratio is one of the most strikingly temperature-dependent features in the spectrum. The 1364-cm^{-1} band intensity, which is unobservable at 88 °K, asymptotically approaches one-half the intensity of the 1358-cm^{-1} band as the temperature approaches 650 °K. The greatest portion of the change occurs between 300 and 500 °K. This change appears to be at least partially due to a decrease in the ν_1 intensity. The decrease could not be definitely established because of a deterioration of the sample optical quality at elevated temperatures. The symmetric stretch mode has a linear temperature dependence of -1.0 ± 0.2 cm^{-1}/100 °K over the full temperature range of the study.

The overtone of the bending mode was studied as a function of temperature by mixing the Raman scattered radiation with light from a hollow-cathode iron-neon lamp. This procedure allowed the measurement of the frequency change with temperature to within ± 0.2 cm^{-1}. The low-temperature (88–300 °K) behavior was found to have a slope of 0.3 cm^{-1}/100 °K. The change in frequency between room temperature and 520 °K was found to be 2.6 cm^{-1} rather than the 0.7 cm^{-1} that would be obtained by extrapolation of the low-temperature behavior.

Iqbal and Garrett[34] have shown a correlation between the instability of the metal azide compound and the magnitude of the lower-frequency bending-mode component. They observed decreasing frequency to correspond to increasing azide instability or sensitivity. More extensive high-temperature examination of the ν_2 mode is needed before the significance of the deviation that we observe can be established in relation to the high-temperature instability of sodium azide.

The most interesting changes that occur in the Raman spectrum are in the low-frequency region. The temperature dependence of the librational mode frequencies is presented in Fig. 10. The E_g mode exhibits linear anharmonic behavior as a function of temperature. Symbol size is representative of the uncertainties of the measurements except at temperatures greater than 400 °K where large half-widths, background, and abbreviated procedure made the uncertainty about twice the symbol size. A linear least-squares fit yields a temperature-dependent change of -4.5 ± 0.1 cm^{-1}/100 °K. The B_g mode in α-sodium azide also exhibits a linear temperature dependence with a slope of 3.2 ± 0.2 cm^{-1}/100 °K. Below approximately 60 °K negligible changes are observed in the A_g and B_g mode frequencies. That is, the structural changes are essentially terminated in the neighborhood of 60 °K.

The librational-mode band half-widths are presented in Fig. 11 as a function of temperature. The half-widths are observed to change with temperature at a linear rate of 4.6 cm^{-1}/100 °K over the range of the study above 100 °K.

The recorded half-widths for the powdered samples which were taken directly from the supplier's container are consistently larger than those of the crystal samples, although the frequencies agree quite well. Grinding a crystal to a particle size similar to that of the powder did not result in larger measured half-widths. One possible explanation is that the larger half-widths observed with the unrefined powder are due to inferior microscopic crystalline structure or impurities. This is plausible in view of the difficulty encountered in growing good single crystals and the phenomenon of twinning which is known to occur.

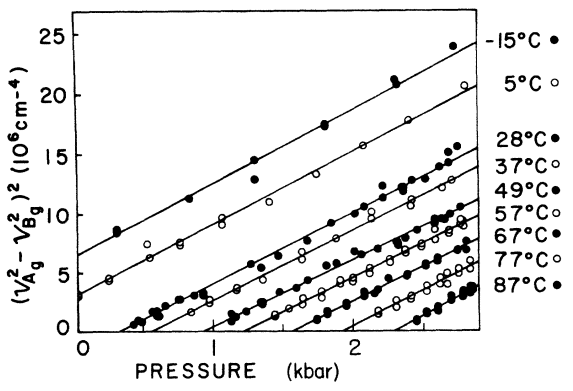

FIG. 9. Librational-mode pressure-dependent frequency splitting and linear least-squares fits to the data.

TABLE V. Least-squares-fit parameters of the librational-mode frequency splitting assuming a pressure dependence of the form $(\nu^2_{A_g} - \nu^2_{B_g})^2 = a + bP$.

T (°C)	a (10^6 cm^{-4})	σ_a (10^6 cm^{-4})	b (10^3 cm^{-4}/bar)	σ_b (10^3 cm^{-4}/bar)	χ^2	$P_c = -a/b$ (kbar)	$\sigma_{(-a/b)}$ (kbar)
−15	6.52	0.38	6.02	0.26	0.68	−1.08	0.08
5	3.15	0.13	5.97	0.15	0.50	−0.53	0.03
28	−1.80	0.08	5.89	0.09	0.53	0.30	0.01
37	−3.12	0.16	5.81	0.12	0.27	0.54	0.03
49	−5.10	0.16	5.54	0.10	0.41	0.92	0.03
57	−6.94	0.17	5.70	0.09	0.27	1.21	0.03
67	−8.99	0.24	5.73	0.12	0.26	1.57	0.06
77	−11.46	0.79	5.90	0.32	0.59	1.94	0.17
87	−14.47	0.84	6.24	0.32	0.40	2.32	0.18

The half-widths are observed to be a linear function of temperature through the region of the phase transition. They are apparently uninfluenced by the transition other than, of course, the appearance of two nondegenerate phonons in the α-phase. The observance of half-width perturbations near the phase transition in the pressure-dependent data but not in the temperature-dependent data is understandable in view of the relative scales of the pressure and temperature dependence of the phase transition.

Temperature-dependent changes in phonon frequencies have contributions from Δ_{AH} as well as Δ_{TE}. In the present treatment, temperature-dependent changes due to Δ_{AH} are taken to be very similar for the A_g and B_g librational modes because of the striking half-width similarities of the modes. Furthermore, the Δ_{TE} terms may be expected to dominate because of the large volume changes which occur. This dominance would minimize the errors introduced by the above approximation. In a manner similar to that of the pressure dependent study, one then again obtains Eq. (4).

The Δ_{TE} term is directly dependent on the lattice strains $\eta_{\alpha\beta}$ making the temperature dependence of the lattice parameters of utmost interest. The actual lattice cell parameters have only been determined at 23 and −95 °C, by fitting of precise x-ray diffractometer data. However, Pringle and Noakes[2] have measured percent changes in lattice plane spacings as a function of temperature using less accurate x-ray powder pattern techniques. Their powder pattern results are represented in Fig. 12 by the solid symbols. Using the 23 and −95 °C lattice cell parameters derived by Pringle and Noakes, we calculated the percent changes in the relevant lattice plane spacings at −100 °C. These quantities are represented in Fig. 12 by open circles.

The observed discrepancies between the open

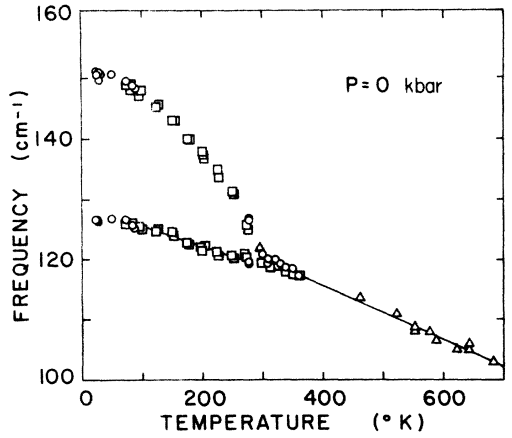

FIG. 10. Librational-mode frequency temperature dependence. Circles and triangles represent single-crystal data. Squares represent powder-sample data.

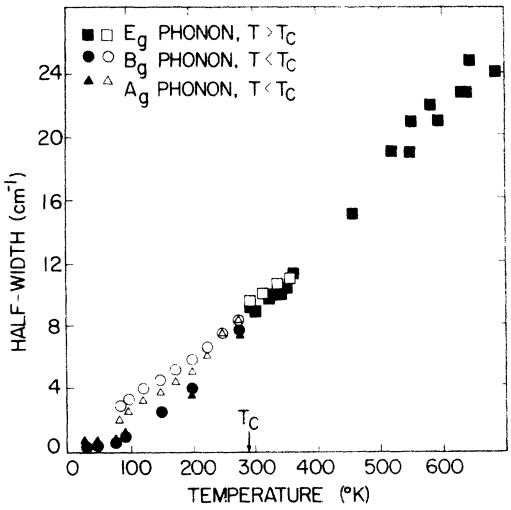

FIG. 11. Temperature-dependent librational-mode half-width data. Open symbols represent powder sample data. Filled symbols represent single-crystal data.

and closed symbols are believed to be predominantly due to the lesser accuracy of the powder pattern measurements. For this reason, proposed models for the cell parameter temperature dependences were fit to the diffractometer results. The assumed general forms of temperature dependences are given by

$$a(T) = a_{23\,^\circ\mathrm{C}} + a'(T_c - T)^{n_a}, \quad b(T) = 3.650\,\text{Å},$$

$$c(T) = c_{23\,^\circ\mathrm{C}} + c'(T_c - T)^{n_c},$$

$$\beta(T) = \beta_{23\,^\circ\mathrm{C}} + \beta'(T_c - T)^{n_\beta},$$

The numerical details of three trial models considered are given in Table VI. Trials I, II, and III correspond to the solid, long-dash and short-dash lines, respectively. This approach does not determine the parameter behavior uniquely but only tests the suitability of various guesses at what the true behavior might be. A more desirable treatment of this problem would involve independent structural analyses at several temperatures. Nevertheless, Fig. 12 illustrates the nearly linear results obtained by assuming that all temperature dependences are of the form $(T_c - T)^{1/2}$.

It will now be shown that such an assumed temperature dependence for the $\eta_{\alpha\beta}$ terms leads to an excellent description of the observed librational mode frequency splitting with temperature. The corresponding $(P - P_c)^{1/2}$ pressure dependence has already been shown to provide a good description of the observed pressure dependent splitting in accordance with the linear temperature-pressure

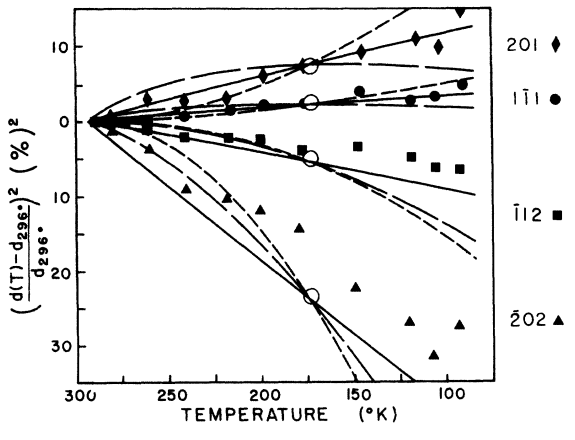

FIG. 12. Percent changes in four monoclinic cell plane spacings as a function of temperature. The filled symbols represent powder-pattern results. The open circles represent the more accurate diffractometer results. The lines indicate calculated plane spacing changes based on three proposed monoclinic cell parameter temperature dependences.

correspondence reported by Pringle and Noakes. From the above assumption and Eq. (4) it follows that

$$(\nu_{A_g}^2 - \nu_{B_g}^2)^2 \propto (T_c - T). \tag{7}$$

The reduced temperature-dependent data and weighted least-square fits are presented in Fig. 13. The high-pressure temperature-dependent data were obtained by interpolation of the pressure-dependent data presented earlier. The corresponding fit parameters, confidence intervals, χ^2 values and extrapolated transition temperatures are presented in Table VII. The data corresponding to temperatures less than 50 °K were neglected in the fitting procedure because of their obvious and expected departure from the behavior of the higher-temperature data. The χ^2 values were found to be less than 1.2 in all cases indicating that the fit parameter confidence intervals are conservative values.

Local heating is an important question to consider when studying the temperature and pressure dependent properties of a crystal using focused laser radiation. Sodium azide offers a unique answer to this question with its own internal "thermometer" in the form of the temperature-dependent librational-mode splitting. Using this "thermometer" a crystal was irradiated at room temperature at a pressure of 172 kbar with focused 4880-Å laser light ranging in power from 100 to 750 mW. The splitting was observed to decrease with increasing laser power at a rate corresponding to a local heating of approximately 1 °K/100 mW. From these results and a comparison of various other measurements, we concluded that local heating amounted to less than 3 °K for all of the pressure- and temperature-dependent measurements and most often was considerably less.

E. Phase transition

One deduction that can be obtained from these measurements is a phase diagram for sodium azide. These results are presented in Fig. 14. The extrapolated zero-splitting pressures are physically unachievable negative values in some cases, but these values are useful for presenting the over-all consistency of the temperature- and pressure-dependent behavior of the librational modes.

The straight line is a least-squares fit to the pressure-dependent data. It has a slope of 33 ± 0.9 bar/°C and a 0 °C intercept of −644 ± 27 bar. This yields an atmospheric pressure transition temperature of (19.5 ± 1.5)°C. This is in agreement with (20 ± 7)°C obtained independently

TABLE VI. Three sets of trial values inserted into the assumed general forms of the monoclinic cell parameter temperature dependences.

Trial No.	n_a	n_c	n_b	a'	c'	β'
I	$\frac{1}{2}$	$\frac{1}{2}$	$\frac{1}{2}$	-0.0100 Å/°K$^{1/2}$	-0.155 Å/°K$^{1/2}$	-0.374 deg/°K$^{1/2}$
II	1	1	$\frac{1}{2}$	-9.17×10^{-4} Å/°K	-1.42×10^{-3} Å/°K	-0.374 deg/°K$^{1/2}$
III	1	1	1	-9.17×10^{-4} Å/°K	-1.42×10^{-3} Å/°K	-03.42×10^{-2} deg/°K

from the temperature-dependence study represented by the open circle in Fig. 14. The relatively greater accuracy of the pressure dependent transition temperature determination is due primarily to refinements made in data acquisition and data analysis after the temperature dependent study was completed. This transition temperature is also consistent with values between 18 and 12 °C obtained by other workers cited earlier. The slope of the line is also similar to the -35 bar/°K dependence observed by Pringle and Noakes[2] between temperature- and pressure-dependent x-ray data.

The ratios of the nine constant-temperature pressure-dependent splitting rates to the 0-bar temperature-dependent rate were calculated. The average of these ratios was found to be -31 bar/°K. This is similar to the ratio obtained from the x-ray measurements and the phase diagram. It lends credence to the assumption made earlier that Δ_{TE} is the important contribution to the splitting.

The B_g librational mode is observed to have a ratio of temperature to pressure-dependent change of -41 bar/°K using the -15 °C data and the 0-bar data. This value is larger than the ratio obtained from the x-ray results and frequency splitting study, as expected, since it includes a contribution from Δ_{AH} in the temperature-dependent behavior. Considering the observed discrepancy, the contribution of $\Delta_{AH}(B_g)$ may be estimated to be approximately 15% of the total change with temperature. The mode Grüneisen constant of the B_g mode is calculated to be 1.5 using the present pressure-dependent data, the temperature-dependent results, and the temperature-pressure correspondence of Pringle and Noakes.[2]

We are aware of no pressure dependent x-ray studies of β-sodium azide, although both Bradley *et al.*[3] and Weir *et al.*[35] have reported some x-ray pressure data on α-sodium azide. Such studies on β-sodium azide would have to be conducted at elevated temperatures. Without such measurements it is not possible to separate the contributions of Δ_{AH} and Δ_{TE} in the β-phase. Using the 87 °C and the 0-bar E_g mode data the temperature/pressure dependence ratio is found to be -40 bar/°K. This value again is large as expected due to the Δ_{AH} contribution that is included. From this and the above observations, the -35 bar/°C presented by Pringle and Noakes can thus be seen to not only be characteristic of the lattice distortion in the α-phase but also of the temperature dependence of the transition pressure, the librational-mode frequency splitting, the B_g-mode frequency behavior, and even the E_g-mode behavior in the β-phase. Assuming a similar Δ_{AH} contribution to the β-phase, this observation leads one to hypothesize a 35 bar/°K pressure temperature correspondence for lattice behavior of β-sodium azide also. These results support the close relationship between the phonon frequency changes and the lattice dimensional configuration changes that we hypothesized for sodium azide.

The half-width behavior is in striking contrast to that of the frequency behavior with the temperature dependence being more significant as expected. The temperature-pressure correspondence in the α-phase is found to be -150 bar/°K and -110 bar/°K for the B_g and A_g modes, respectively, using the 5 °C and 0-bar data. The behavior in the β-phase is 1.2 kbar/°K using the 87 °C and 0-bar data.

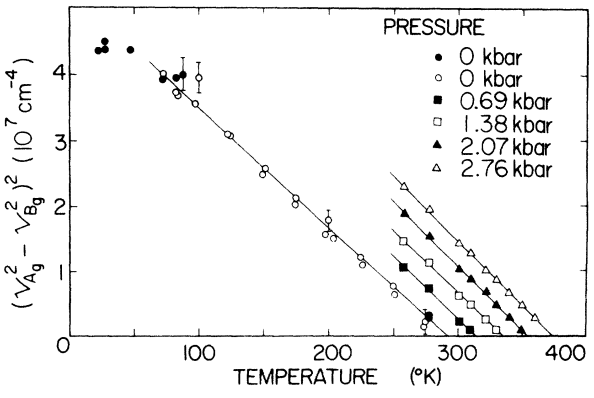

FIG. 13. Librational-mode temperature dependence and linear least-squares fits to the data. The open circles correspond to powder-sample data. All other symbols represent single-crystal data.

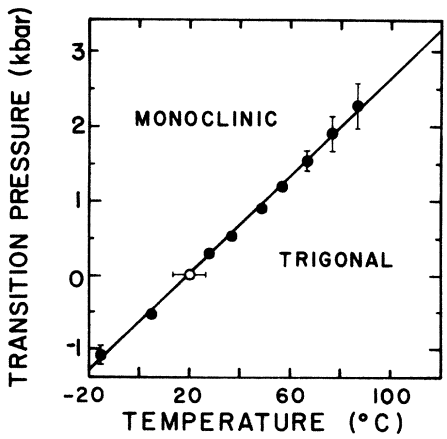

FIG. 14. Sodium-azide phase diagram obtained from extrapolated pressure-dependent (solid circles) and temperature-dependent (open circles) librational-mode zero-frequency splitting.

It is also of interest to note that

$$\frac{(d\nu_{B_g}/dT)_\alpha}{(d\nu_{E_g}/dT)_\beta}=0.71\,,\quad \frac{(dV/dT)_\alpha}{(dV/dT)_\beta}=0.58\,.$$

The volume temperature dependence is taken from the data of Pringle and Noakes[2] and Parsons and Yoffe.[13] Coupling these figures with the earlier temperature-pressure correspondence, we are led to the conjecture that the compressibility of α-sodium azide is 60–70% of that of β-sodium azide. Confirmation of these extrapolations of the present results must await pressure dependent x-ray studies at elevated temperatures.

An investigation of the librational modes for $k\neq 0$ would be of interest in relation to the phase transition. Also, there is the possibility of coupling between the [001] transverse acoustic and librational modes. Such a study could best be done by inelastic neutron scattering, but unfortunately sufficiently large single crystals have thus far not been available. Information about the sodium azide $k\neq 0$ phonons might be obtainable from Raman scattering from crystals with broken translational symmetry.

In summary, the sodium azide phase transition does not conform with either the standard displacive or order-disorder type of second-order transition, although the lattice changes involved occur smoothly and continuously over an appreciable pressure and temperature range. The temperature and pressure behavior, as indicated by the Raman-active E_g phonon as it splits into A_g and B_g modes, indicates that the lattice changes have a second-order-type dependence in the α-phase. The behavior of these phonons in the α phase and in the β-phase is not inconsistent with an order-disorder transition and a slightly disordered β-phase. However, these data, while supporting this hypothesis, are not conclusive because of the undetermined behavior in the immediate vicinity of the transition point.

Note added in proof. Subsequent to the submission of this paper we have become aware of a publication by Zafar Iqbal, J. Chem. Phys. 59, 1769 (1973), which addresses some of the measurements which we are reporting. It is of interest to note that his results are in substantial agreement with our own where overlap exists.

ACKNOWLEDGMENTS

We wish to thank S. Robertson for the design and assembly of the pressure cell, P. A. Temple for making his low-temperature zero-pressure powder-sample data available, and G. E. Pringle for communicating unpublished x-ray and modeling results. We wish to thank S. S. Mitra for an informative conversation concerning his unpublished infrared high-pressure measurements. The able assistance of F. Zutavern with regard to the computer analysis of the data is also much appreciated.

TABLE VII. Least-squares-fit parameters of the librational mode frequency assuming a temperature dependence of the form $(\nu_{A_g}^2-\nu_{B_g}^2)^2=a+bT$.

P (10^3lb/in^2)	a (10^6 cm^{-4})	σ_a (10^6 cm^{-4})	b (10^3 cm^{-4}/°K)	σ_b (10^3 cm^{-4}/°K)	χ^2	$T_c=a/b$ (°K)	σ (°K)
0	53.2	0.8	−182	3	0.58	293	7
10	60.9	3.0	−194	10	0.79	314	22
20	64.8	1.1	−193	3	0.16	336	8
30	71.2	1.0	−201	3	0.20	354	7
40	75.0	0.5	−201	2	0.40	373	4

*Supported in part by the Office of Naval Research Contract No. N00014-68-A-0504.

†Present address: Harry Diamond Laboratories, Branch 320, Connecticut Ave. and Van Ness St., Washington, D. C. 20438.

[1]R. H. Bartram and P. K. Jain, Phys. Rev. B 7, 3878 (1973).
[2]G. E. Pringle and D. E. Noakes, Acta Crystallogr. B 24, 262 (1968).
[3]R. S. Bradley, J. D. Grace, and D. C. Munro, Z. Kirstallogr. 120, 349 (1964).
[4]S. B. Hendricks and L. Pauling, J. Am. Chem. Soc. 47, 2904 (1925).
[5]R. Loudon, Adv. Phys. (G.B.) 13, 424 (1964).
[6]W. G. Penny and G. B. Sutherland, Proc. R. Soc. A 156, 678 (1936).
[7]J. I. Bryant, J. Chem. Phys. 40, 3195 (1964).
[8]T. A. Richter, M. L. Malhotra, and K. D. Mollar, Mater. Res. Bull. 5, 203 (1970).
[9]S. S. Mitra (private communications) quoted by Ref. 10.
[10]H. A. Rafizadeh, S. Yip, and H. Prask, J. Chem. Phys. 56, 5377 (1972).
[11]L. D. Landau and E. M. Liftshitz, *Statistical Physics* (Pergamon, London, 1962).
[12]B. S. Miller and G. J. King, J. Chem. Phys. 39, 2779 (1964).
[13]R. B. Parson and A. D. Yoffe, Phys. Chem. Solids 20, 36 (1966).
[14]H. P. Fritzer and K. Torkar, Monatsh. Chem. 97, 703 (1966).
[15]J. D. Campbell and C. K. Coogan, J. Chem. Phys. 44, 2075 (1966).
[16]E. D. Stevens and H. Hope, American Crystallography Association Summer Meeting, N10, Iowa State University, Ames, Iowa, 1971 (unpublished).
[17]G. E. Pringle (private communication).
[18]P. Temple and C. E. Hathaway, Phys. Rev. B 7, 3685 (1973).
[19]C. E. Hathaway and L. A. Rahn, Rev. Sci. Instrum. 43, 294 (1972).
[20]T. J. Lewis, Trans. Faraday Soc. 62, 889 (1966).
[21]N. R. Draper and H. Smith, *Applied Regression Analysis* (Wiley, New York, 1966).
[22]J. I. Bryant and R. L. Brooks III, J. Chem. Phys. 43, 880 (1965).
[23]J. I. Bryant, J. Chem. Phys. 45, 689 (1966).
[24]J. I. Bryant and R. L. Brooks, J. Chem. Phys. 54, 5315 (1971).
[25]R. Savoie and M. Pézolet, Can. J. Chem. 45, 1677 (1967).
[26]C. E. Hathaway and P. A. Temple, Phys. Rev. B 3, 3479 (1971).
[27]P. A. Temple and C. E. Hathaway, Bull. Am. Phys. Soc. 15, 298 (1970).
[28]G. J. Simonis and C. E. Hathaway, Bull. Am. Phys. Soc. 17, 497 (1972).
[29]J. M. Worlock, *Structural Phase Transitions and Soft Modes*, edited by E. J. Samuelsen, E. Anderson, and J. Feder (Universitetsforlaget, Oslo, Norway, 1971).
[30]Z. Iqbal, L. H. Sarma, and K. D. Möller, J. Chem. Phys. 57, 4728 (1972).
[31]M. Couzi, J. B. Sokoloff, and C. H. Perry, J. Chem. Phys. 58, 2965 (1973).
[32]R. A. Cowley, Rep. Prog. Phys. 31, 123 (1968).
[33]P. Gray, Q. R. Chem. Soc. 17, 441 (1963).
[34]Z. Iqbal and W. Garrett, J. Chem. Phys. 55, 4528 (1971).
[35]C. S. Weir, S. Block, and G. J. Piermarini, J. Chem. Phys. 53, 4265 (1970).